






## STUDY OF DEFECT STRUCTURE OF SILICON DOPED WITH DYSPROSIUM USING X-RAY PHASE ANALYSIS AND RAMAN SPECTROSCOPY

 Khodjakbar S. Daliev<sup>a</sup>,  Sharifa B. Utamuradova<sup>b</sup>,  Jonibek J. Khamdamov<sup>b</sup>,  
 Shahriyor B. Norkulov<sup>b\*</sup>,  Mansur B. Bekmurotov<sup>b</sup>

<sup>a</sup>Branch of the Federal State Budgetary Educational Institution of Higher Education “National Research University MPEI”,  
1 Yogdu st., Tashkent, Uzbekistan

<sup>b</sup>Institute of Semiconductor Physics and Microelectronics at the National University of Uzbekistan,  
20 Yangi Almazar st., Tashkent, 100057, Uzbekistan

\*Corresponding Author e-mail: [nshb19990@gmail.com](mailto:nshb19990@gmail.com)

Received August 16, 2024; revised October 15, 2024; accepted October 25, 2024

In this paper, the effect of doping silicon with dysprosium (Dy) on its structural and optical characteristics is investigated. Silicon n-Si was doped with dysprosium by thermal diffusion at 1473 K for 50 h. Raman spectroscopy and X-ray diffraction analysis were used for the analysis. The Raman spectroscopy results showed a main peak at 523.93 cm<sup>-1</sup>, corresponding to n-Si optical phonons, with an increase in the intensity and full width at half maximum (FWHM) in n-Si<Dy> samples, indicating an improvement in the crystallinity of the structure. A decrease in the intensity of the peaks at 127.16 cm<sup>-1</sup> and 196.24 cm<sup>-1</sup>, associated with amorphous structures, confirms a decrease in defects. The detection of a new peak at 307.94 cm<sup>-1</sup> indicates successful deposition of dysprosium as nanocrystallites associated with the 2TA phonon mode in the cubic phase of Dy<sub>2</sub>O<sub>3</sub>. X-ray diffraction analysis revealed characteristic structural lines indicating the (111) crystalline orientation and the presence of microdistortions in the lattice. Heat treatment and rapid cooling lead to a change in the intensity of structural lines, an increase in the second- and third-order lines, which indicates microstrains and a change in the size of subcrystallites. Doping of silicon with dysprosium improves the crystallinity of the structure, reduces the number of defects and forms polycrystalline layers on the surface consisting of SiO<sub>2</sub> and Dy<sub>2</sub>O<sub>3</sub> nanocrystals.

**Key words:** Silicon; Defects; Dysprosium; Rare earth element; Raman spectroscopy; Diffusion; Heat treatment; Temperature; Composition; X-ray phase analysis

**PACS:** 33.20.Rm, 33.20.Fb

### INTRODUCTION

It is known that defect formation processes are significantly affected by various factors [1-6]. The formation efficiency and annealing kinetics of certain defects in the bulk of silicon depend on the presence of various active and inactive uncontrolled impurities, their content and state in the silicon lattice, other specially introduced impurities, the presence of several impurities at once, and many factors. Diffusion is carried out from the oxide film of rare earth elements on the surface of the silicon wafer. Thin-film nanocomposites consisting of crystalline and amorphous Si nanoparticles embedded in silicon oxide layers have been widely studied over the past two decades as suitable materials for non-volatile memory devices, third-generation photovoltaic devices, and other applications. The efficiency of rare earth doping in silicon and the manifestation of optical properties of the structures depend on the spectrum of optically and electrically active centers containing rare earth elements, their total concentration, and the interaction with uncontrolled impurities and thermal defects in the bulk of the material. Recent advances in self-aligned silicide deposition have revived the interest in metal-oxide semiconductor Schottky barrier field-effect transistors (SB-MOSFETs), and devices with outstanding electrical characteristics and high-frequency performance have been fabricated. Metal silicides such as PtSi, DySi<sub>2-x</sub>, YbSi<sub>2-x</sub>, and ErSi<sub>2-x</sub> have been extensively studied as Schottky barrier source-drain (S/D) contacts due to their low Schottky barrier height on silicon [7-8].

Raman spectroscopy has proven its effectiveness in monitoring the local formation of various technologically important metal silicides (e.g. CoSi<sub>2</sub>, TiSi<sub>2</sub>, PtSi and NiSi) [2-9]. The Raman spectrum also provides a unique “fingerprint” of the material: each phonon in the spectrum corresponds to a unique vibrational mode of the crystal lattice. This method provides additional information such as the phase state, strain, nucleation site and grain size of the silicide material.

The aim of this work is to dope n-Si silicon with dysprosium (Dy) by the diffusion method at a temperature of 1473 K and to study the structural and optical characteristics of n-Si silicon samples and the REE oxide film on the surface of n-Si<Dy> silicon wafer using Raman spectroscopy and X-ray diffraction (XRD) analysis.

### MATERIALS AND METHODS

In this study, n-Si and its doped n-Si<Dy> sample were analyzed using Raman spectroscopy (RS) and X-ray diffraction (XRD) methods. Control n-Si samples with initial resistance from 0.2 to 100 Ω×cm was selected for the experiment. The doping process with dysprosium (Dy) was carried out by thermal diffusion method. The samples were chemically cleaned and treated with HF solution to remove oxide layers from the surface.

Then Dy (99.999% purity) was deposited on the cleaned silicon surface in a high vacuum environment with a vacuum level of  $10^{-6}$  to  $10^{-7}$  Torr in evacuated quartz ampoules using an oil-free vacuum pump system. Diffusion annealing of the samples was performed at a temperature of 1473 K for 50 hours, followed by rapid and slow cooling to uniformly distribute the material and achieve the maximum concentration of dysprosium in silicon.

Raman spectroscopy was performed on a QE Pro High-Sensitivity Spectrometer Raman microscope at room temperature using a 532 nm laser in the wavelength range from 50 to 1200  $\text{cm}^{-1}$ . X-ray diffraction analysis was performed on a MiniFlex II diffractometer (Rigaku, Japan) using  $\text{CuK}\alpha$  radiation. All diffraction patterns were recorded in the angular range  $2\theta=3\div 120^\circ$ . The obtained diffraction data were analyzed for the presence of characteristic signals for n-Si<Dy> composites. The presence of elements was determined based on literature data on phases and the ICDD card database for known compounds.

## RESULTS AND DISCUSSIONS

To study the physical and chemical structure of the samples, Raman analysis was performed, the obtained spectra are presented in Figure 1.

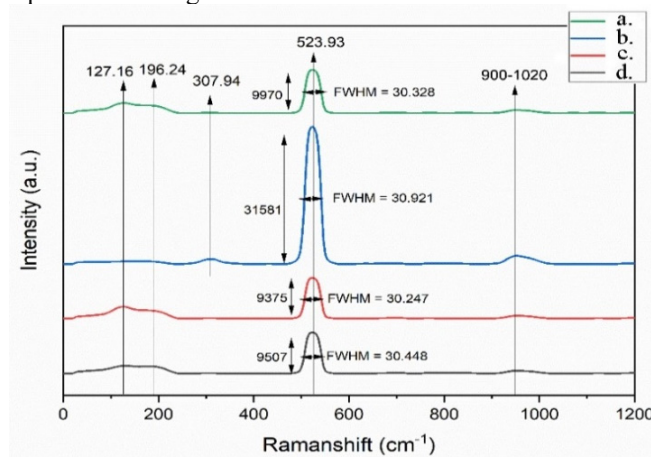


**Figure 1.** Raman spectra of the studied samples:  
**a.** n-Si doped with dysprosium (<Dy>), heat-treated at 1373 K for 50 hours, followed by rapid cooling and 15  $\mu\text{m}$  depth removal; **b.** n-Si doped with dysprosium (<Dy>), heat-treated at 1373 K for 50 hours, followed by rapid cooling; **c.** n-Si (control), heat-treated at 1373 K for 50 hours, followed by rapid cooling; **d.** n-Si (original material)

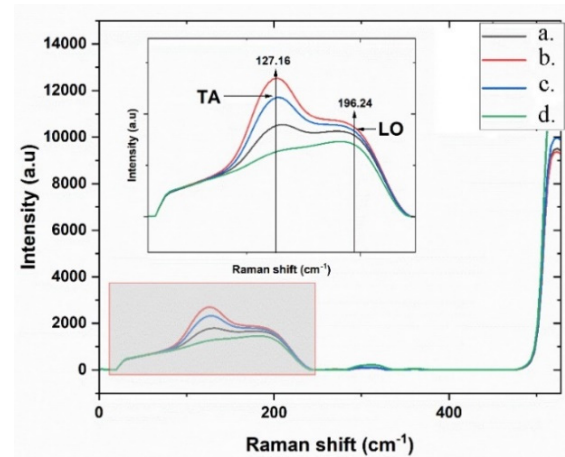


**Figure 2.** TA and LO peaks of samples:  
**a.** n-Si (as-is). **b.** n-Si (control) heat-treated at 1373 K for 50 h followed by rapid cooling; **c.** n-Si doped with dysprosium (<Dy>) heat-treated at 1373 K for 50 h followed by rapid cooling and 15  $\mu\text{m}$  depth removal; **d.** n-Si doped with dysprosium (<Dy>) heat-treated at 1373 K for 50 h followed by rapid cooling

As shown in Figure 1, the first-order Raman spectrum (G point,  $k\sim 0$ ) of all single-crystal silicon samples at room temperature is observed at  $523.93\text{ cm}^{-1}$  [10, 11]. The peak is formed as a result of optical phonon scattering inside the n-Si nanocrystal, which corresponds to the LO (longitudinal optical) and TO (transverse optical) optical phonon modes of n-Si at the center of the Brillouin zone [12]. It is known that tensile stress causes the Raman peak to shift toward a lower wavenumber, while compressive stress causes the Raman peak to shift toward a higher wavenumber [13]. Figures 1 and 2 show the typical shifts of Raman peaks for amorphous silicon based on the experimental results of references, which are approximately  $127.16\text{ cm}^{-1}$  (phonon mode similar to TA-like phonon mode) and  $196.24\text{ cm}^{-1}$  (phonon mode similar to LA-like phonon mode) [12, 13, 16].

It is evident from Fig. 1 that the peak intensity and first-order bandwidth at half-maximum for the heat-treated n-Si<sub>ht</sub> sample are lower than that obtained for the control sample (n-Si). In addition, the higher intensity of the peaks at  $127.16\text{ cm}^{-1}$  and  $196.24\text{ cm}^{-1}$  appearing in the Raman spectrum of the heat-treated sample indicates that the amorphous silicon with higher concentration of crystal defects is formed during the processing.

According to the Raman spectra of the obtained n-Si<Dy> samples, due to the deposition of dysprosium on the n-Si surface, the peak intensity significantly increased along with the FWHM value at  $523.93\text{ cm}^{-1}$ , and the peak intensity of the amorphous structures at  $127.16\text{ cm}^{-1}$  and  $196.24\text{ cm}^{-1}$  sharply decreased. These observations indicate that the deposition of dysprosium leads to an increase in the crystallinity of the structure and a decrease in the defect sites in the n-Si samples. In addition, a new peak appearing at  $307.94\text{ cm}^{-1}$  is associated with the Fg band (2TA phonon mode) in the cubic phase of  $\text{Dy}_2\text{O}_3$  [17, 18]. The peak position, intensity and width at half maximum are  $307.94\text{ cm}^{-1}$ , 1157.84 and  $44.15\text{ cm}^{-1}$ , respectively. Thus, using Raman spectroscopy, it is possible to prove the successful deposition of dysprosium (in the form of n-Si<Dy>) on the silicon surface for 50 hours at a temperature of 1473 K under vacuum conditions.

After removing the 15  $\mu\text{m}$  thick surface, it is seen that the intensity of the  $\text{Dy}_2\text{O}_3$  peak decreases significantly at about  $307.94\text{ cm}^{-1}$ , and the intensity of the crystalline and amorphous structure decreases and increases, respectively, compared to n-Si. When analyzing the n-Si<Dy> sample, the removal of the  $\text{Dy}_2\text{O}_3$  layer from the surface of the silicon wafer was determined.

Fig. 3 shows the secondary phonon range of 15  $\mu\text{m}$  thick samples obtained as a result of mechanical processing by diffusing Dy atoms onto the n-Si surface after heat treatment (phonon mode similar to 2TO) [12.14.15.]. In the range of 900-1020  $\text{cm}^{-1}$ , there is a broad peak, which is formed as a result of the superposition of two or more optical modes [19.].

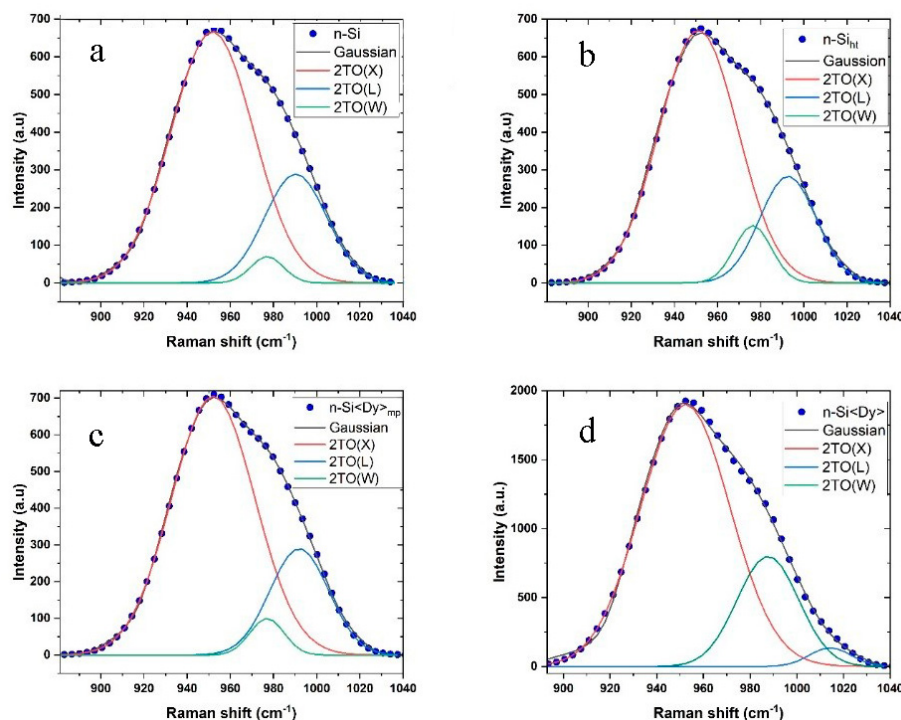


**Figure 3.** Second-order phonon range of samples:

**a.** n-Si (as-received material). **b.** n-Si (control) heat-treated at 1373 K for 50 h followed by rapid cooling; **c.** n-Si doped with dysprosium (<Dy>), heat-treated at 1373 K for 50 h followed by rapid cooling and 15  $\mu\text{m}$  depth removal; **d.** n-Si doped with dysprosium (<Dy>), heat-treated at 1373 K for 50 h followed by rapid cooling

For a deep study of the obtained Raman spectra of the samples, work was carried out to separate the obtained signals (3 peaks 2TO(X), 2TO(W) and 2TO(L)) using the Origin Pro and Fityk programs; the obtained data on these peaks are presented in Table 1.

**Table 1.** Results of the Raman spectra analysis of Si samples.

No	Samples studied	2TO	Center ( $\text{cm}^{-1}$ )	Area	Height	FWHM
1	n-Si	X	951.64	31939.7	666.817	44.9978
		L	990.27	289.095	33.8002	33.8002
		W	977.02	1327.96	70.3974	17.7213
2	n-Si <sub>ht</sub>	X	951.16	30764.9	670.615	43.0974
		L	992.65	9270.74	283.238	30.7489
		W	976.35	3285.26	152.592	20.2259
3	n-Si<Dy> <sub>mp</sub>	X	952.03	34169.9	705.095	45.5265
		L	991.93	9885.45	290.036	32.0194
		W	976.94	1983.78	99.8088	18.6721
4	n-Si<Dy>	X	952.23	91713.8	1901.56	45.1889
		L	1014.27	3032.63	136.081	20.9358
		W	987.64	26456.7	799.234	31.0977

Comparing the obtained Raman spectra data of the samples (Table 1), we can draw a conclusion on the effect of various treatments and additives on the properties of the materials. Below is a comparison of n-Si<Dy> samples with the control n-Si sample:

#### Change in the 2TO(X) peak shift:

thermally treated n-Si<sub>ht</sub> sample: the area decreased by  $\sim 3.7\%$  compared to the control sample (31939.7 versus 30764.9), the height remained virtually unchanged (666.817 versus 670.615), the half-width decreased by  $\sim 4.2\%$  (44.9978 versus 43.0974).

sample obtained by decreasing the sample surface area by 15  $\mu\text{m}$  n-Si<Dy><sub>mp</sub>: area increase by  $\sim 7\%$  (31939.7 vs. 34169.9), height increase by  $\sim 5.8\%$  (666.817 vs. 705.095), half-maximum increase by  $\sim 1.2\%$  (44.9978 vs. 45.5265). The area and height increase, but the rate of increase is significantly lower than that of the n-Si<Dy> sample.

n-Si<Dy> sample: area increased by ~187% (31939.7 vs. 91713.8), height increased by ~185% (666.817 vs. 1901.56), width at half-maximum increased by ~0.4% (44.9978 vs. 45.1889).

**Change in 2TO(L) peak shift:**

thermally treated n-Siht sample: area increased by ~3106% (289.095 vs. 9270.74), height increased by ~738% (33.8002 vs. 283.238), width at half-width is ~9% lower (33.8002 vs. 30.7489).

sample obtained by decreasing the sample surface by 15 μm n-Si<Dy>mp: area increased by ~3321% (289.095 vs. 9885.45), height increased by ~758% (33.8002 vs. 290.036), width at half-width is ~5.3% lower (33.8002 vs. 32.0194).

n-Si<Dy> sample: area increased by ~949% (3032.63 vs. 289.095), height increased by ~302% (136.081 vs. 33.8002), FWHM decreased by ~38% (20.9358 vs. 33.8002).

**Change in 2TO(W) peak shift:**

thermally treated n-Siht sample: area increased by ~147% (1327.96 vs. 3285.26), height increased by ~116% (70.3974 vs. 152.592), FWHM increased by ~14% (17.7213 vs. 20.2259).

sample obtained by decreasing the sample surface area by 15 μm n-Si<Dy>mp: area increased by ~49% (1327.96 vs. 1983.78), height increased by ~42% (70.3974 vs. 99.8088), FWHM increased by ~5.4% (17.7213 vs. 18.6721).

n-Si<Dy> sample: area increased by ~1894% (1327.96 vs. 26456.7), height increased by ~1035% (70.3974 vs. 799.234), FWHM increased by ~75% (17.7213 vs. 31.0977). Raman scattering can also be used to determine the thickness of our silicide films. This is done by measuring the attenuation of Raman scattering on silicon substrate phonons due to the silicide layer. The intensity of the silicon peak is determined by the following equation:

$$I = I_0 e^{-2\alpha d}, \tag{1}$$

where,  $I_0$  is the intensity of the reference silicon wafer without the top layer,  $\alpha$  is the absorption coefficient of the top layer,  $d$  is the film thickness [17]. To determine the yield thickness, equation (1) can be rewritten as follows:

$$\alpha d = -1/2 \ln (I/I_0). \tag{2}$$

We measured two vibrations of dysprosium monosilicide at wavelengths of 127 and 196  $\text{cm}^{-1}$ . To deeply study the physical and chemical structure of both the control n-Si sample and the obtained n-Si<Dy> samples, X-ray phase analysis was performed.

Figure 4 shows the X-ray diffraction pattern of the n-Si sample (initial). It is evident from the data presented in Figure 4 that the X-ray diffraction pattern contains some structural reflections with different intensities (the structural data are presented in Table 2).

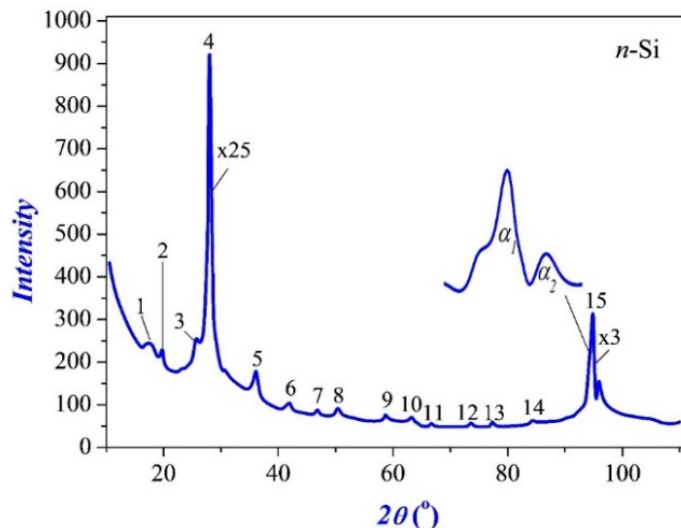


**Figure 4.** X-ray diffraction pattern of n-Si sample (initial)

Among such structural reflections, the structural line observed at  $2\theta = 27.99^\circ$  with  $d/n = 3188$  nm has the highest intensity; it was established based on the experimental analysis that it belongs to the crystallographic orientation (111). The high intensity of this reflection ( $21779 \text{ imp}\cdot\text{sec}^{-1}$ ) and the half-width (0.01 rad), determined from the experimental results, indicate both a good degree of crystallinity of the studied samples and the fact that most of the constituent atoms are arranged in the crystallographic order (111). According to this structural reflection, its beta ( $\beta$ ) component was observed at  $2\theta = 25.31^\circ$  with  $d/n = 3.5096$  nm, and its second (222) and third (333) orders were observed at  $2\theta = 57.9^\circ$  with  $d/n = 1.5933$  nm and  $2\theta = 94.68$  with  $d/n = 1.0474$ , respectively. Usually, the second (222) order reflex is considered to be a forbidden structural line with respect to the crystallographic first order (111), and in most cases it manifests itself in the X-ray diffraction pattern by the presence of microdistortions of the crystal lattice. The ratio of the intensity of the

structural lines to the intensity of the main structural line is  $I(222)/I(111) = 3.6 \cdot 10^{-3}$ , and this value is greater than  $10^{-4}$ , which once again confirms the presence of microdistortions in the crystal lattices of the studied n-Si sample (initial). Such microdistortions of the crystal lattice are formed as a result of the uneven distribution of oxygen atoms from the main background impurities of silicon-based structures. Also, the presence of microdistortions in the crystal lattice is indicated by the fact that the inelastic background level of the X-ray diffraction pattern has a non-monotonic character, i.e. it takes variable values at small, medium and large scattering angles.

In turn, these microdistortions (formed as a result of filling several oxygen atoms in the crystal lattice with unsaturated silicon-oxygen bonds) lead to the formation of a thin layer on the surface of the n-Si plate, belonging to another phase group. Therefore, several structural lines (structural data are given in Table 2), corresponding to silicon dioxide, are observed in the X-ray diffraction pattern at small and medium scattering angles.

**Table 2.** Structural data of n-Si (initial)

N <sub>2</sub>	Reflexes and background level	Intensive in rel. units	Location 2 $\theta$ , deg	Interlayer distance, d, Å	Line width, rad	Block size, nm
1	Diffuse. Neg. SiO <sub>x</sub> ; x < 2	247	17.1	5.11	0.05	0.9
2	(100) <sub>SiO<sub>2</sub></sub>	233	20.4	4.354	0.009	17.6
3	(111) <sub>β</sub>	231	25,31	3,5096	-	-
4	(111) <sub>Si</sub>	21779	27.997	3,1843	0.01	14.21
5	(210) <sub>SiO<sub>2</sub></sub>	176	35,39	2,45403	0,018	8.44
6	(200) <sub>SiO<sub>2</sub></sub>	99.5	41.66	2.1662	0.017	9.29
7	(220) <sub>Si</sub>	88	46.57	1.9489	0.01	15.3
8	(212) <sub>SiO<sub>2</sub></sub>	99.6	49.84	1.8285	0.015	13.9
9	(222) <sub>Si</sub>	80	57,9	1,5933	Prohibited	
10	(300) <sub>SiO<sub>2</sub></sub>	60.1	64.2	1.451	0.018	9.49
11	(301) <sub>SiO<sub>2</sub></sub>	69	66.2	1.411	0.022	7.92
12	(302) <sub>SiO<sub>2</sub></sub>	74	73.8	1.2828	0.02	8.43
13	(331) <sub>Si</sub>	74	77.14	1.234	0.016	11.56
14	(333,511) <sub>β</sub>	72	83.97	1.1515-	-	-
15	(333,511) <sub>Si</sub>	1221	94.68	1.0474	0.027	7.86
Inelastic background						
	Small-angle scattering	259	-	-	-	-
	Medium-angle scattering	75	-	-	-	-
	High-angle scattering	58	-	-	-	-

The parameters of the crystal lattices were determined using the experimental values of these structural reflections based on the formulas given in [20], they are equal to  $a = b = 4.9762$  nm and  $c = 5.4321$  nm, respectively. This fact proves that their unit cell belongs to the trigonal crystal lattice and the space group  $P3_21$ . Based on the obtained results and their analysis, as well as the values of the SiO<sub>2</sub> crystallite sizes presented in Table 2 and their different crystallographic directions, it can be concluded that a polycrystalline layer with a thickness of  $1 \div 2$  μm is formed on the surface of the studied n-Si samples. Also, clear splitting by  $\alpha_1$  and  $\alpha_2$  radiations (having two times differences from each other) of the third (333) structural reflection on the X-ray diffraction pattern indicates that a layer is formed on the surface of the sample under the influence of microstresses.

In addition, the X-ray diffraction pattern at  $2\theta \approx 17.1^\circ$  shows a wide (FWHM = 0.05 rad) diffuse reflection caused by structural fragments of SiO<sub>x</sub> in the surface layers with unsaturated bonds. The too wide width of this reflection indicates that the sizes of the structural fragments caused by this reflection are small and there is no long-range order in their arrangement. Consequently, these structural fragments are not SiO<sub>x</sub> nanocrystals, but clusters. The characteristic sizes of these clusters were  $\sim 0.9$  nm, respectively.

Based on the experimental values of the main (111) structural reflection, it was determined that the lattice parameter of the n-Si plate under study was  $a_{Si} = 5.4451$  nm.

The samples, the structural values of which were determined above, were subjected to heat treatment at a temperature of 1100°C for 40 hours, and then cooled at a cooling rate of 3000C/s. The surface of such plates was polished using certain technological means. X-ray structural studies of the processed samples were carried out, the experimental results are shown in Fig. 5.

From Fig. 5 it is evident that the X-ray patterns of the processed n-Si plates differ significantly from the X-ray pattern of the original samples (Fig. 4) and an increase in the intensity of structural lines by 13 times is observed in it. However, the scattering angle of the observed main structural reflection (111) remained practically unchanged, and the lattice constant is equal to  $a_{Si(pol)} = 5.4456$  nm with a very small difference ( $\Delta a = 0.0005$  nm) in values.

Also, the characteristic second (222) and third (333) orders increase by 114 and 377 times, respectively. In most X-ray diffraction patterns of the undistorted diamond-like structure lattice, the second (222) order structural line is not observed (forbidden reflection), and the intensity of the third (333) order structural line is lower than the intensity of the main structural line (111) [21]. In our case, the X-ray diffraction pattern showed high-intensity second (222) and third (333) order structural lines. This, in turn, indicates that certain microdeformations arose in their crystal lattice due to long-

term (40 hours) heat treatment (1100 °C) and subsequent rapid cooling of the samples. In support of our statement, we can cite an example of the ratio  $I(222)/I(111)$  of the intensities of the lines of the second (222) order and the main (111) structure, equal to  $3.4 \cdot 10^{-2}$ . The fact that this value is almost 100 times greater than the value of  $10^{-4}$  indicates the presence of sufficient microstresses in the crystal lattice [22]. In addition, the sharp cooling of the samples caused the disintegration of their subcrystallites, which led to a decrease in their sizes (Table 3). A decrease in the size of the subcrystallites leads to an increase in the number of boundary areas in them, this fact, in turn, causes an increase in the number of defective high-potential regions, i.e. microdistortions at their interfaces [20].

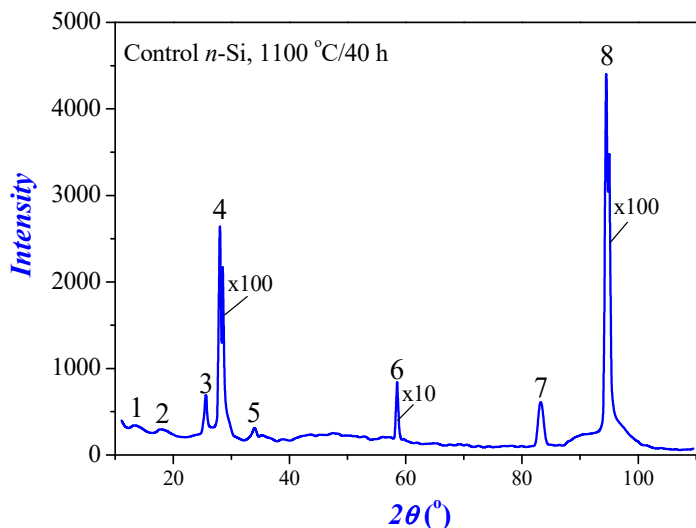


Figure 5. X-ray diffraction pattern of processed n-Si wafers (control)

Table 3. Structural data of processed n-Si wafers (control)

№	Reflexes and background level	Intensive in rel. units	Location 2θ, deg	Interlayer distance, d, Å	Line width, rad	Block size, nm
1	Diffuse. Neg. SiO <sub>x</sub> ; x < 2	347	13.51	6.5484	0.1473	0.99
2	Diffuse. Neg. SiO <sub>x</sub> ; x < 2	296	17.84	5.0103	0.1499	0.98
3	(111) <sub>β</sub>	689	25.47	3.4964	-	-
4	(111) <sub>Si</sub>	268610	27.995	3.1846	0.017	8.8
5	(210) <sub>SiO<sub>2</sub></sub>	313	34.14	2.5531	0.024	6.3
6	(222) <sub>Si</sub>	9175	58.47	1.5772	Prohibited	
7	(333,511) <sub>β</sub>	636	83.24	1.1597	-	-
8	(333,511) <sub>Si</sub>	461190	94.5	1.0492	0.017	12.4
Inelastic background						
	Small-angle scattering	219	-	-	-	-
	Medium-angle scattering	132	-	-	-	-
	High-angle scattering	63	-	-	-	-

After heat treatment, the surface of the samples was polished and a 2 μm thick layer was removed. When analyzing the obtained sample, only one structural line was observed on their X-ray diffraction pattern at  $2\theta = 34.14^\circ$  with  $d/n = 2.5531$  nm, belonging to silicon dioxide, corresponding to a trigonal crystal lattice (with parameters  $a = b = 4.9762$  nm and  $c = 5.4321$  nm) and space group P321. This, in turn, indicates that under the influence of heat treatment, oxygen atoms form a bond with silicon atoms at a certain depth, and then under the influence of rapid cooling they form crystallites. But due to the ionic radius of oxygen ( $r_{Si^{4+}} = 1.40 \text{ \AA}$ ), which is greater than the ionic radius of silicon ( $r_{O^{2-}} = 0.42 \text{ \AA}$ ), its ions prefer to be located along the unsaturated bond at the boundaries of subcrystallites [23]. This nature of oxygen leads to the formation of structural fragments with low symmetry among subcrystallites consisting of silicon ions with high symmetry, as well as to deformations of the crystal lattice due to the arrangement of its atoms in the nodes. This is evidenced by an increase in the level of the inelastic background at small, medium and large scattering angles of the X-ray diffraction patterns of the studied samples and the observation of two diffuse reflections associated with SiO<sub>x</sub> fragments in small-angle scattering (see Fig. 5).

Subsequently, using doping (for 40 hours at a temperature of 1100 °C) with Dy atoms, n-Si<Dy> samples were obtained. The obtained X-ray diffraction data for the samples are shown in Fig. 6.

It is evident that the X-ray diffraction pattern of n-Si<Dy> platinum differs sharply from the X-ray diffraction pattern of the n-Si sample (initial sample, Fig. 4). It is necessary to take into account the fact that the intensity of the main structural line (111) did not change, and the intensity of the structural lines of the second (222) and third (333) orders increased by 1.6 and 82 times, respectively. Observation of the forbidden structural line of the second (222) order and the ratio of its intensity to the intensity of the main (111) reflection is  $I(222)/I(111) = 4.8 \cdot 10^{-3}$  and this value is less than  $10^{-4}$ . Also, the intensity of the line of the structure of the third (333) order is 4.5 times greater than the intensity of the main reflection (111). This, in turn, indicates that volume defects were formed at the boundaries of subcrystallites as a result of prolonged heat treatment of the samples and rapid cooling at the end of the process [24]. In addition, in the X-ray diffraction pattern, the main (111) structural line was shifted toward higher-angle scattering ( $\Delta\theta = 0.18^\circ$ ). Based on the results of experiments on this structural line, it was established that the lattice constant of the sample is  $a_{\text{Si}<\text{Dy}>} = 5.4186$  nm. This, in turn, is associated with the doping of the silicon plate with Dy atoms, and the difference in the ionic radii of the O ( $r_o^{-2} = 1.3 \text{ \AA}$ ) and Dy ( $r_{\text{Dy}}^{3+} = 0.91 \text{ \AA}$ ) atoms with Si ( $r_{\text{Si}}^{4+} = 0.42 \text{ \AA}$  and  $r_{\text{Si}}^{-4} = 2.7 \text{ \AA}$ ) indicates that a deformation equal to  $a_{\text{Si}} - a_{\text{Si}<\text{Dy}>} = 0.026$  nm has formed in the crystal lattice.

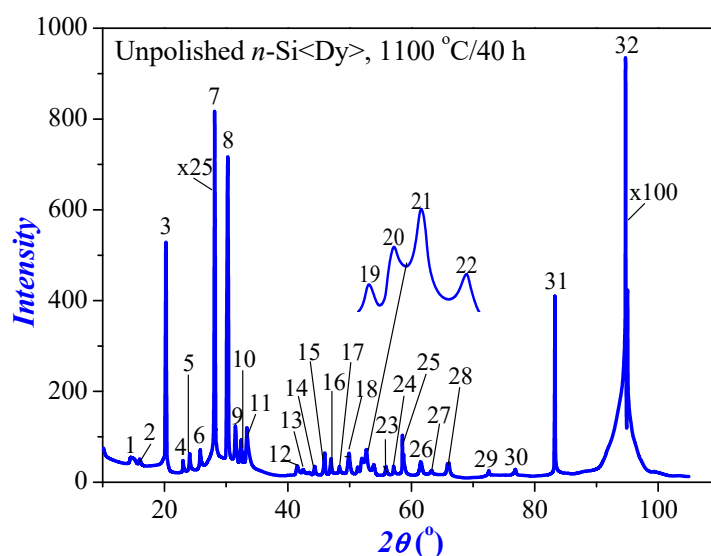


Figure 6. Radiograph of unpolished n-Si<Dy> platins

In addition, a number of structural reflections belonging to other crystallographic orientations are observed in the X-ray diffraction pattern with small- and medium-angle scattering, and their experimental and calculated data are presented in Table 4. Based on the analysis of the obtained results, it was found that these structural reflections are observed as a result of combinations of the mutual order of the  $\text{SiO}_2$  and  $\text{Dy}_2\text{O}_3$  compounds. As a result of long-term heat treatment of the samples, the diffusing Dy atoms combine with oxygen atoms from the main background impurities of silicon to form nanocrystallites. This is evidenced by the fact that the inelastic background level tends to be monotonous in the medium and large-angle scattering in the X-ray diffraction pattern of the obtained n-Si<Dy> sample. Also, after the processes carried out, as a result of sharp cooling of the samples, it was found that nanocrystallites based on  $\text{SiO}_2$  and  $\text{Dy}_2\text{O}_3$  compounds accumulate mainly in the surface areas of the obtained sample and form oxide layers with polycrystalline properties. Based on the experimental results of the study of the formed layer, consisting of nanocrystallites of different crystallographic orientation and size, it was established that such a layer has a monoclinic unit cell with parameters  $a = b = 6.4548$  nm and  $c = 8.6549$  nm, belonging to the space group  $P2_{1/c}$ .

However, rapid cooling of the samples leads to the formation of unsaturated bonds due to the absence of oxygen and dysprosium atoms in the ordered arrangement of silicon-oxygen-dysprosium atoms of some nanocrystallites [25, 23]. This, in turn, leads to the formation of small clusters consisting of a small number of atoms [26]. The small size and close arrangement of such clusters leads to the appearance of diffuse reflection in small-angle scattering X-ray diffraction patterns of the studied samples.

Table 4. Structural data without polished n-Si<Dy> wafers

No	Reflexes and background level	Intensive in rel. units	Location $2\theta$ , deg	Interlayer distance, $d$ , $\text{\AA}$	Line width, rad	Block size, nm
1	Diffuse. Neg. $\text{SiDy}_x\text{O}_x$ ; $x < 2$	54	14.56	6.057	0.09	1.6
2	$(110)_{\text{SiO}_2+\text{Dy}_2\text{O}_3}$	51	15.89	5.575	0.0054	27
3	$(200)_{\text{SiO}_2+\text{Dy}_2\text{O}_3}$	535	20.18	4.3964	0.0033	44.5
4	$(111)_{\text{SiO}_2+\text{Dy}_2\text{O}_3}$	48	22.79	3.8989	0.0035	42.1
5	$(210)_{\text{SiO}_2+\text{Dy}_2\text{O}_3}$	67	23.88	3.7264	0.0035	42.3

No	Reflexes and background level	Intensive in rel. units	Location 2θ, deg	Interlayer distance. d, Å	Line width, rad	Block size, nm
6	(111) <sub>β</sub>	86	26.02	3.4207	-	-
7	(111) <sub>Si</sub>	22178	28.13	3.1688	0.003	49.7
8	(021) <sub>SiO<sub>2</sub>+Dy<sub>2</sub>O<sub>3</sub></sub>	1067	29.41	3.0337	0.0041	36.4
9	(300) <sub>SiO<sub>2</sub>+Dy<sub>2</sub>O<sub>3</sub></sub>	842	30.74	2.9059	0.0041	36.6
10	(121) <sub>SiO<sub>2</sub>+Dy<sub>2</sub>O<sub>3</sub></sub>	110	32.25	2.7733	0.0036	41.8
11	(22 $\bar{1}$ ) <sub>SiO<sub>2</sub>+Dy<sub>2</sub>O<sub>3</sub></sub>	147	33.27	2.6946	0.0037	40.6
12	(130) <sub>SiO<sub>2</sub>+Dy<sub>2</sub>O<sub>3</sub></sub>	25	40.48	2.2263	0.0053	29.1
13	(031) <sub>SiO<sub>2</sub>+Dy<sub>2</sub>O<sub>3</sub></sub>	38	41.39	2.1796	0.0062	24.9
14	(230) <sub>SiO<sub>2</sub>+Dy<sub>2</sub>O<sub>3</sub></sub>	35	44.29	2.0431	0.0053	29.5
15	(321) <sub>SiO<sub>2</sub>+Dy<sub>2</sub>O<sub>3</sub></sub>	65	45.87	1.9766	0.0053	29.7
16	(220) <sub>Si</sub>	59	46.93	1.938	0.004	39.5
17	(13 $\bar{2}$ ) <sub>SiO<sub>2</sub>+Dy<sub>2</sub>O<sub>3</sub></sub>	37	48.29	1.8852	0.0017	93.3
18	(411) <sub>SiO<sub>2</sub>+Dy<sub>2</sub>O<sub>3</sub></sub>	73	49.86	1.8272	0.0074	21.57
19	(51 $\bar{1}$ ) <sub>SiO<sub>2</sub>+Dy<sub>2</sub>O<sub>3</sub></sub>	40	51.26	1.7808	0.0057	28.17
20	(500) <sub>SiO<sub>2</sub>+Dy<sub>2</sub>O<sub>3</sub></sub>	62	51.94	1.7588	0.0068	23.68
21	(41 $\bar{3}$ ) <sub>SiO<sub>2</sub>+Dy<sub>2</sub>O<sub>3</sub></sub>	85	52.65	1.7369	0.0076	21.25
22	(231) <sub>SiO<sub>2</sub>+Dy<sub>2</sub>O<sub>3</sub></sub>	44	53.8	1.7025	0.0081	20.04
23	(311) <sub>Si</sub>	39	55.73	1.6478	0.0024	68.23
24	(004) <sub>SiO<sub>2</sub>+Dy<sub>2</sub>O<sub>3</sub></sub>	46	56.94	1.6156	0.0042	39.21
25	(222) <sub>Si</sub>	131	58.46	1.5774	Prohibited	
26	(24 $\bar{2}$ ) <sub>SiO<sub>2</sub>+Dy<sub>2</sub>O<sub>3</sub></sub>	48	61.27	1.5116	0.007	24
27	(142) <sub>SiO<sub>2</sub>+Dy<sub>2</sub>O<sub>3</sub></sub>	30	63.29	1.4681	0.0065	46.9
28	(43 $\bar{3}$ ) <sub>SiO<sub>2</sub>+Dy<sub>2</sub>O<sub>3</sub></sub>	49	65.81	1.4179	0.0072	23.9
29	(31 $\bar{5}$ ) <sub>SiO<sub>2</sub>+Dy<sub>2</sub>O<sub>3</sub></sub>	29	72.46	1.3031	0.0059	30.4
30	(350) <sub>SiO<sub>2</sub>+Dy<sub>2</sub>O<sub>3</sub></sub>	31	76.64	1.2422	0.0039	47.3
31	(333,511) <sub>β</sub>	444	83.25	1.1595	-	-
32	(333,511) <sub>Si</sub>	100210	94.68	1.0474	0.0017	125.7
Inelastic background						
Small-angle scattering		31	-	-	-	-
Medium-angle scattering		14	-	-	-	-
High-angle scattering		11	-	-	-	-

Fig. 7 shows an X-ray diffraction pattern after polishing the obtained n-Si samples doped with Dy atoms at a temperature of 1100°C for 40 hours. Significant differences can be seen in the resulting X-ray diffraction pattern compared to the X-ray diffraction patterns of the original samples (Fig. 4).

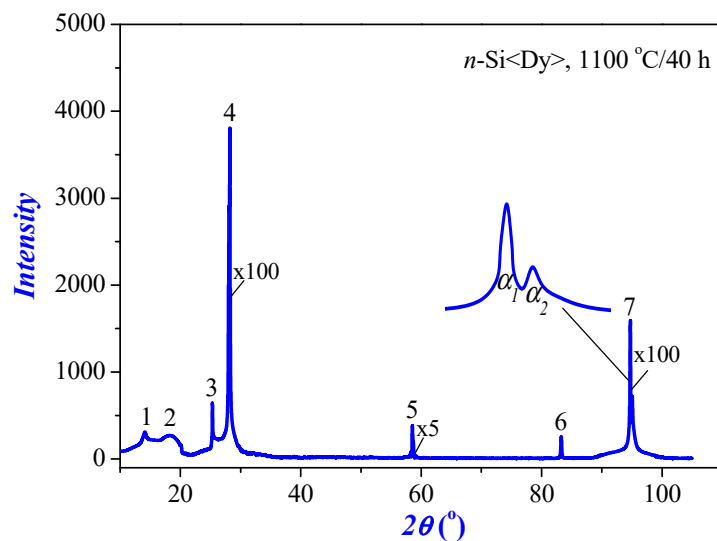


Figure 7. X-ray diffraction pattern of processed n-Si<Dy> samples

It can be seen that the main (111) structural line is 18 times higher than its intensity and is shifted toward higher scattering angles at  $\Delta\theta = 0.19^\circ$  (Table 5). This, in turn, indicates that the number of atoms belonging to a certain crystallographic orientation increase, i.e. the degree of monocrystallization increases [22]. But the manifestation shifted toward higher angular scattering reports that the deformation caused by the penetration of Dy atoms into the silicon crystal



lattice resulted in the formation of  $a_{\text{Si}} - a_{\text{Si(pol)<Dy>}} = 5.4451 \text{ nm} - 5.4080 \text{ nm} = 0.037 \text{ nm}$ . This, in turn, leads to the fact that in the X-ray diffraction pattern the radiation intensity of the second (222) (forbidden) order structure increases by 25 times. The intensity ratio of this structural line to the intensity of the main (111) structural line is  $I(222)/I(111) = 0.005$ , and this value is greater than  $10^{-4}$  and this indicates the presence of micronutrients under the influence of deformations [27].

When studying the sample (333), the structural line was observed to be two times less intense compared to the intensity of the main structural line (111), and was also clearly split into  $\alpha_1$  and  $\alpha_2$  components and suggested a ratio of their intensities of  $I_{\alpha_1}/I_{\alpha_2} \approx 2$ . This, in turn, indicates that Dy atoms cannot be located in bulk crystal nodes due to the difference in the ionic radius of Dy atoms Dy ( $r_{\text{Dy}^{3+}} = 0,91 \text{ \AA}$ ) and Si ( $r_{\text{Si}^{4+}} = 0.42 \text{ \AA}$  and  $r_{\text{Si}^{4+}} = 2.7 \text{ \AA}$ ), i.e., they settle on the nodes at the interfaces of subcrystallites and surface areas. This is also evidenced by the fact that the level of the inelastic background of the X-ray diffraction pattern has a monotonic character with medium- and large-angle scattering.

The obtained research data led to the following conclusion: silicon, oxygen and dysprosium atoms form new bonds, forming different crystallites as a result of long-term heat treatment of the samples. Also, sharp cooling of the samples after heat treatment leads to the formation of oxide layers on the surface areas of the formed crystallites. However, as a result of polishing the surface of the samples and removing layers  $1\div 2 \mu\text{m}$  thick, no structural lines associated with  $\text{SiO}_2$  and  $\text{Dy}_2\text{O}_3$  compounds were observed in the X-ray diffraction patterns of the n-Si(pol)<Dy> samples. Only in scattering at an angle of  $14.05^\circ$  with  $d/n = 6.2774$  was a structural line associated with the  $\text{Dy}_2\text{O}_3$  compound observed, which means that oxygen and dysprosium atoms are located in empty sites at the interfaces of the n-Si(pol)<Dy> sample subcrystallites. This allows the formation of small-sized nanocrystallites due to the accumulation of impurity atoms in these places. Based on the experimental results of the structural reflection  $(001)_{\text{Dy}_2\text{O}_3}$ , it was established that such nanocrystallites belong to the space group P4m2 and consist of tetragonal unit cells with parameters  $a = b = 3.8116 \text{ nm}$  and  $c = 5.4933 \text{ nm}$ , respectively.

**Table 5.** Structural data of processed n-Si<Dy> wafers

N <sub>o</sub>	Reflexes and background level	Intensive in rel. units	Location 2 $\theta$ , deg	Interlayer distance. d, $\text{\AA}$	Line width, rad	Block size, nm
1	$(001)_{\text{Dy}_2\text{O}_3}$	337	14.05	6.2774	0.011	13.2
2	Diffuse. Neg. $\text{SiDy}_x\text{O}_x; x < 2$	288	18.27	4.8669	0.1297	0.98
3	$(111)_\beta$	4360	25.33	3.5121	-	-
4	$(111)_{\text{Si}}$	398650	28.19	3.1626	0.0049	52.3
5	$(222)_{\text{Si}}$	2056	58.53	1.5757	Prohibited	
6	$(333,511)_\beta$	261	83.29	1.1591	-	-
7	$(333,511)_{\text{Si}}$	193840	94.68	1.04747	0.0071	97.6
Inelastic background						
	Small-angle scattering	38	-	-	-	-
	Medium-angle scattering	15	-	-	-	-
	High-angle scattering	11	-	-	-	-

In addition, at the boundaries of subcrystallite division near the surface areas of the Si(pol)<Dy> sample, the formation of unsaturated bonds with oxygen and dysprosium atoms is observed, and these do not allow the atoms to be located in a long-range order. As a result, diffuse reflection is observed during small-angle scattering of the sample under study.

## CONCLUSIONS

The study included a comprehensive assessment of the structural and optical characteristics of dysprosium (Dy) doped silicon using Raman spectroscopy and X-ray diffraction (XRD) analysis. The aim of the work was to study the effects of dysprosium doping of silicon by high-temperature diffusion and their influence on the crystal structure and optical properties of the materials.

Raman spectroscopy showed that doping with dysprosium leads to significant changes in the Raman spectrum. In particular, an increase in the peak intensity at  $523.93 \text{ cm}^{-1}$  and the appearance of a new peak at  $307.94 \text{ cm}^{-1}$  associated with the phonon modes of  $\text{Dy}_2\text{O}_3$  were noted. This indicates successful deposition of dysprosium on the silicon surface and an increase in the crystallinity of the structure, as well as a decrease in the defect concentration. At the same time, the observed decrease in the intensity of the peaks corresponding to amorphous silicon confirms the improvement of the crystalline structure of the samples. X-ray phase analysis confirmed changes in the silicon crystal lattice after doping. In particular, a change in the crystal lattice parameters associated with the introduction of dysprosium is observed. The intensities of the X-ray lines for the samples subjected to heat treatment increased, indicating the formation of new crystalline phases and the possible formation of oxide layers.

Based on the X-ray phase analysis data, the exact crystallographic orientation and change in the lattice parameters depending on the treatment were established. Thus, in the n-Si<Dy> samples, changes were found indicating the presence

of dysprosium dioxides and a change in the crystal structure of silicon, which is confirmed by shifts in the X-ray peaks and changes in the sizes of subcrystallites.

In general, the results of the work show that doping silicon with dysprosium leads to an improvement in the crystal structure and a change in the optical properties. The use of Raman spectroscopy and X-ray phase analysis methods made it possible to better understand the mechanisms of interaction of rare earth elements with silicon and their effect on the properties of semiconductor materials.

#### ORCID

- © Khodjakbar S. Daliev, <https://orcid.org/0000-0002-2164-6797>; © Sharifa B. Utamuradova, <https://orcid.org/0000-0002-1718-1122>  
© Jonibek J. Khamdamov, <https://orcid.org/0000-0003-2728-3832> © Shahriyor B. Norkulov, <https://orcid.org/0000-0002-2171-4884>;  
© Mansur B. Bekmuratov, <https://orcid.org/0009-0006-3061-1568>

#### REFERENCES

- [1] A.I. Prostomolotov, Yu.B. Vasiliev, and A.N. Petlitsky, "Mechanics of defect formation during growth and heat treatment of single-crystal silicon," (4), 1716–1718 (2011). [http://www.unn.ru/pages/e-library/vestnik/19931778\\_2011\\_-4-4\\_unicode/147.pdf](http://www.unn.ru/pages/e-library/vestnik/19931778_2011_-4-4_unicode/147.pdf)
- [2] Sh.B. Utamuradova, Sh.Kh. Daliyev, J.J. Khamdamov, Kh.J. Matchonov, Kh.Y. Utemuratova, *East Eur. J. Phys.* (2), 274-278 (2024). <https://doi.org/10.26565/2312-4334-2024-2-28>
- [3] K.S. Daliev, S.B. Utamuradova, J.J. Khamdamov, and Z.E. Bahronkulov, "Electrophysical properties of silicon doped with lutetium," *Advanced Physical Research*, 6(1), 42–49 (2024). <https://doi.org/10.62476/apr61.49>
- [4] Kh.S. Daliev, Sh.B. Utamuradova, J.J. Khamdamov, and M.B. Bekmuratov, "Structural Properties of Silicon Doped Rare Earth Elements Ytterbium," *East Eur. J. Phys.* (1), 375-379 (2024). <https://doi.org/10.26565/2312-4334-2024-1-37>
- [5] K.S. Daliev, S.B. Utamuradova, A. Khaitbaev, J.J. Khamdamov, S.B. Norkulov, and M.B. Bekmuratov, "Defective Structure of Silicon Doped with Dysprosium," *East European Journal of Physics*, (2), 283-287 (2024). <https://doi.org/10.26565/2312-4334-2024-2-30>
- [6] S.B. Utamuradova, K.S. Daliev, A.I. Khaitbaev, J.J. Khamdamov, J.S. Zarifbayev, and B.S. Alikulov, "Defect Structure of Silicon Doped with Erbium," *East European Journal of Physics*, (2), 288-292 (2024). <https://doi.org/10.26565/2312-4334-2024-2-31>
- [7] S.B. Utamuradova, S.K. Daliev, A. Khaitbaev, J. Khamdamov, U.M. Yuldoshev, and A.D. Paluanova, "Influence of Gold on Structural Defects of Silicon," *East European Journal of Physics*, (2), 327-335 (2024). <https://doi.org/10.26565/2312-4334-2024-2-38>
- [8] R.T.-P. Lee, K.-M. Tan, T.-Y. Liow, C.-S. Ho, S. Tripathy, G.S. Samudra, D.-Z. Chi, and Y.-C. Yeo, "Probing the ErSi<sub>1.7</sub> Phase Formation by Micro-Raman Spectroscopy," *Journal of The Electrochemical Society*, 154(5) H361-H364 (2007). <https://doi.org/10.1149/1.2710201>
- [9] J. Kedzierski, P. Xuan, E.H. Anderson, J. Bokor, T.J. King, and C. Hu, "Complementary silicide source/drain thin-body MOSFETs for the 20 nm gate length regime," in: *International Electron Devices Meeting 2000. Technical Digest. IEDM (Cat. No. 00CH37138)* (San Francisco, CA, USA, 2000), p. 57-60. <https://doi.org/10.1109/IEDM.2000.904258>
- [10] W.-J. Lee, and Y.-H. Chang, "Growth without Postannealing of Monoclinic VO<sub>2</sub> Thin Film by Atomic Layer Deposition Using VCl<sub>4</sub> as Precursor," *Coatings*, 8, 431 (2018). <https://doi.org/10.3390/coatings8120431>
- [11] K. Ali, S. Khan, M. Zubir, and M.Z.M. Jafri, "Spin-on doping (SOD) and diffusion temperature effect on re-combinations/ideality factor for solar cell applications," *Chalcogenide Letters*, 9, 457–463 (2012). [https://www.chalcogen.ro/457\\_KhuramAli.pdf](https://www.chalcogen.ro/457_KhuramAli.pdf)
- [12] V. Mankad, S. Gupta, P. Jha, N. Ovsyuk, and G. Kachurin, "Low-frequency Raman scattering from Si/Ge nanocrystals in different matrixes caused by acoustic phonon quantization," *J. Appl. Phys.* 112, 54318 (2012). <https://doi.org/10.1063/1.4747933>
- [13] T. Liu, P. Ge, and W. Bi, "The Influence of Wire Speed on Phase Transitions and Residual Stress in Single Crystal Silicon Wafers Sawn by Resin Bonded Diamond Wire Saw," *Micromachines (Basel)*, 12, (2021). <https://doi.org/10.3390/mi12040429>
- [14] G.-W. Lee, Y.-B. Lee, D.-H. Baek, J.-G. Kim, and H.-S. Kim, "Raman Scattering Study on the Influence of E-Beam Bombardment on Si Electron Lens," *Molecules*, 26, (2021). <https://doi.org/10.3390/molecules26092766>
- [15] K. Adu, M. Williams, M. Reber, R. Jayasingha, H.R. Gutierrez, and G. Sumanasekera, "Probing Phonons in Nonpolar Semiconducting Nanowires with Raman Spectroscopy," *J. Nanotechnol.* 2012, 264198 (2012). <https://doi.org/10.1155/2012/264198>
- [16] Y. Gogotsi, C. Baek, and F. Kirscht, "Raman microspectroscopy study of processing-induced phase transformations and residual stress in silicon," *Semicond. Sci. Technol.* 14, 936 (1999). <https://doi.org/10.1088/0268-1242/14/10/310>
- [17] D. Casimir, H. Alghamdi, I.Y. Ahmed, R. Garcia-Sanchez, and P. Misra, "Raman Spectroscopy of Graphene, Graphite and Graphene Nanoplatelets," in: *2D Materials*, edited by C. Wongchoosuk, and Y. Seekaew, (IntechOpen, 2019). <https://doi.org/10.5772/intechopen.84527>
- [18] K. Maex, and M. Van Rossum, "Properties of Metal Silicides," *Inspec*, (The institution of Electrical Engineers, London, UK, 1995), p. 5. <https://api.semanticscholar.org/CorpusID:92679751>
- [19] Sh.B. Utamuradova, Kh.J. Matchonov, J.J. Khamdamov, and Kh.Y. Utemuratova, "X-ray diffraction study of the phase state of silicon single crystals doped with manganese," *New Materials, Compounds and Applications*, 7(2), 93-99 (2023). [http://jomardpublishing.com/UploadFiles/Files/journals/NMCA/v7n2/Utamuradova\\_et\\_al.pdf](http://jomardpublishing.com/UploadFiles/Files/journals/NMCA/v7n2/Utamuradova_et_al.pdf)
- [20] S.Z. Zainabidinov, Sh.B. Utamuradova, et al., "Structural Peculiarities of the (ZnSe)<sub>1-x-y</sub>(Ge<sub>2</sub>)<sub>x</sub>(GaAs<sub>1-δ</sub>Bi<sub>δ</sub>)<sub>y</sub> Solid Solution with Various Nano-inclusions," *Journal of Surface Investigation: X-ray, Synchrotron and Neutron Techniques*, 16(6), 1130–1134 (2022). <https://doi.org/10.1134/S1027451022060593>
- [21] I.L. Shulpina, R.N. Kyutt, V.V. Ratnikov, I.A. Prokhorov, I.Zh. Bezbakh, M.P. Shcheglov, "Methods of X-ray diffraction diagnostics of heavily doped semiconductor single crystals," *Journal of Technical Physics*, 80(4), 105 (2010). <https://journals.ioffe.ru/articles/viewPDF/9970>
- [22] S.Z. Zainabidinov, A.S. Saidov, M.U. Kalanov, and A.Y. Boboev, "Synthesis, Structure and Electro-Physical Properties n-GaAs-p-(GaAs)<sub>1-x-y</sub>(Ge<sub>2</sub>)<sub>x</sub>(ZnSe)<sub>y</sub> Heterostructures," *App. Sol. Energy*, 55(5), 291–308 (2019). <https://doi.org/10.3103/S0003701X1905013X>
- [23] K.V. Ravi, *Imperfections and Impurities in Semiconductor Silicon*, (Wiley, New York, 1981).

- [24] A.N. Tereshchenko, Dislocation luminescence in silicon with different impurity composition, PhD Thesis, Chernogolovka, 2011.
- [25] M.A. Lourenço, Z. Mustafa, W. Luduczak, L. Wong, R.M. Gwilliam, and K.P. Homewood, "High temperature dependence Dy<sup>3+</sup> in crystalline silicon in the optical communication and eye-safe spectral regions," *Optics Letters*, **38**(18), 3669-3672 (2013). <https://doi.org/10.1364/OL.38.003669>
- [26] I.P. Suzdalev, and P.I. Suzdalev, "Nanoclusters and nanocluster systems. Organization, interaction, properties," *Advances in Chemistry*, **70**(3), 203-240 (2001). <https://doi.org/10.1070/RC2001v070n03ABEH000627>
- [27] N.V. Gokhfeld, Electron microscopic study of atomically ordered alloys based on Cu-Pd and Cu-Au, subjected to severe plastic deformation and subsequent annealing, PhD Thesis, Ekaterinburg, 2019. <http://elar.urfu.ru/handle/10995/95084>

**ДОСЛІДЖЕННЯ ДЕФЕКТНОЇ СТРУКТУРИ КРЕМНІЮ, ЛЕГОВАНОВОГО ДИСПРОЗІЄМ, ЗА ДОПОМОГОЮ РЕНТГЕНОФАЗОВОГО АНАЛІЗУ ТА РАМАНІВСЬКОЇ СПЕКТРОСКОПІЇ**

**Ходжакбар С. Далієв<sup>а</sup>, Шаріфа Б. Утамурадова<sup>б</sup>, Джонібек Дж. Хамдамов<sup>б</sup>,  
Шахрійор Б. Норкулов<sup>б</sup>, Мансур Б. Бекмуратов<sup>б</sup>**

<sup>а</sup>*Філія Федерального державного бюджетного навчального закладу вищої освіти «Національний дослідницький університет МПЕІ», вул. Йогду, 1, м. Ташкент, Узбекистан*

<sup>б</sup>*Інститут фізики напівпровідників та мікроелектроніки Національного університету Узбекистану, 100057, Ташкент, Узбекистан, вул. Янги Алмазар, 20*

У даній роботі досліджено вплив легування кремнію диспрозієм (Dy) на його структурні та оптичні характеристики. Кремній n-Si легували диспрозієм методом термодифузії при 1473 K протягом 50 годин. Для аналізу використовували спектроскопію комбінаційного розсіювання та рентгеноструктурний аналіз. Результати рамановської спектроскопії показали головний пік при 523,93 см<sup>-1</sup>, що відповідає оптичним фононам n-Si, зі збільшенням інтенсивності та повної ширини на половині максимуму (FWHM) у зразках n-Si<Dy>, що вказує на покращення в кристалічність структури. Зменшення інтенсивності піків при 127,16 см<sup>-1</sup> і 196,24 см<sup>-1</sup>, пов'язаних з аморфними структурами, підтверджує зменшення дефектів. Виявлення нового піку при 307,94 см<sup>-1</sup> вказує на успішне осадження диспрозію у вигляді нанокристалів, пов'язаних із фононою модою 2TA у кубічній фазі Dy<sub>2</sub>O<sub>3</sub>. Рентгеноструктурний аналіз виявив характерні структурні лінії, що вказують на орієнтацію кристала (111) та наявність мікроспотворень у ґратці. Термічна обробка та швидке охолодження призводять до зміни інтенсивності структурних ліній, збільшення ліній другого та третього порядку, що свідчить про мікродеформації та зміну розмірів субкристалів. Легування кремнію диспрозієм покращує кристалічність структури, зменшує кількість дефектів і формує на поверхні полікристалічні шари, що складаються з нанокристалів SiO<sub>2</sub> і Dy<sub>2</sub>O<sub>3</sub>.

**Ключові слова:** кремній; дефекти; диспрозій; рідкоземельний елемент; Раманівська спектроскопія; дифузія; тепла обробка; температура; композиція; рентгенофазовий аналіз